The Interaction of a Supernova Remnant with a Pulsar Wind Bubble

Dargan M. Frierson
Department of Physics, North Carolina State University, Raleigh, NC 27695-8202

ABSTRACT

This is a summary of work done so far investigating the interaction between the pulsar wind bubble and the reverse shock of a supernova remnant, specifically applied to the Vela supernova remnant. We have performed many one-dimensional hydrodynamics simulations, and several two-dimensional simulations of this scenario: the pulsar nebula is modeled as a γ=4/3, low density bubble, and the outer gas is a γ=5/3 thermal gas whose density, pressure, and velocity profiles are determined from supernova parameters and the analytic solution for a self-similar driven wave (s=0, n=9). Data from these simulations is presented through space-time diagrams of density for the one-dimensional simulations and density and pressure plots for the 2-D. Approximations for the synchrotron emissivity are made using a few simple assumptions; these are then transformed into images comparable to observations using a line-of-sight integration routine. We investigate the possibility that the filamentary structure seen in the center of the remnant is directly caused by the reverse shock interacting with the pulsar wind bubble. Presented here are our preliminary results, problems, and questions regarding the numerical simulations.

Subject headings: supernova remnants, pulsars, Vela

1. Introduction

Recent observations of the Vela supernova remnant (SNR) in both radio and X-ray have brought about various theories to explain the main features of the system. In the center of the system is Vela X, a pulsar nebula with a flat radio spectral index (Weiler and Panagia 1980;Dwarakanath 1991). The radio emission is characterized by filamentary structure (Frail et al. 1997). The morphological differences between the central pulsar nebula and the outer shell have caused Bock, Turtle, and Green (Bock, Turtle, and Green 1998 to propose the Vela SNR as the Galactic archetype for the composite class of remnants.

The main controversy as to the nature of this SNR is the fact that the pulsar is displaced from the center of the remnant. Markwardt and Ögleman (Markwardt and Ögleman 1995) suggested that an X-ray filament extending from the pulsar to the south is produced by a jet, which has also accelerated the pulsar to its current position. It has not yet been determined whether this

X-ray filament is thermal or nonthermal (Markwardt and Ögleman 1997). One of the radio filaments was initially thought to be associated with this X-ray feature (Frail et al. 1997), but higher resolution scans have shown that this filament is similar to the other filaments of Vela X (Bock, Turtle, and Green 1998). Further, the X-ray spectrum is similar to that of the more diffuse X-ray emission in the area (Markwardt and Ögleman 1997). Wijers and Sigurdsson (Wijers and Sigurdsson 1997) also have discounted the jet theory because the momentum of the jet is much too large as compared to the spin-down momentum loss rate. However, as an alternative theory, they suggested that the filament is caused by fallback onto the neutron star and a trail left by a high velocity binary companion.

This theory has many difficulties in it though, so we investigate the more likely possibility that the radio structure and perhaps also the X-ray feature are caused by the reverse shock interacting with the pulsar wind bubble. At this time in a pulsar-driven remnant's life ($\sim 10^4$ years), the pulsar's input has dropped steeply, and the pulsar nebula expands more or less adiabatically. At around this same time, the bulk of the stellar ejecta has reached the reverse shock, and with nothing driving into it, the reverse shock begins to propogate inwards. Reynolds and Chevalier (Reynolds and Chevalier 1983) have derived an expression for the time it takes for this reverse shock to return to the center based on supernova parameters. Using this formula for Vela, the possibility of recent interactions with a reverse shock is supported by the accepted estimates for the remnant's age ($\sim 10^4$ years).

In this model, the displacement of Vela X from being centered on the pulsar is the result of an asymmetric reverse shock wave. The radio filaments are the result of turbulent motions brought about by the interaction between the thermal gas and the pulsar nebula. Strectching of magnetic field lines may give linear features. The X-ray feature may also be a result of this interaction. We run numerical hydrodynamics simulations with a varying gamma to model this situation, and perform synchrotron visualizations using approximations.

2. Model

We use the numerical hydrodynamics code VH-1, run on SGI workstations and supercomputers at the North Carolina Supercomputing Center to perform the simulations. VH-1 is a Lagrangian-remap version of the piecewise parabolic method developed by Colella and Woodward (Collela and Woodward 1984). The original version was written and tested by the Numerical Astrophysics Group the Virginia Institute for Theoretical Astrophysics. The updated version that allows for variable adiabatic index gamma among other changes was written by Blondin.

We begin with one-dimensional simulations of the Vela remnant, assuming spherical symmetry. We then proceed to two-dimensional models that let us view the instabilities and the effects thereof. We proceed with a detailed description of the initial conditions for the model.

2.1. The Bubble

The pulsar wind bubble, composed of relativistic gas, is modeled as a γ=4/3 fluid. The density in this area is much lower than anything else on the grid, but large enough so that the Courant time step, which is inversely proportional to the sound speed in the medium, does not become too small. We know the sound speed of this relativistic fluid should be close to c/3. As describre in Section 3.3, we ran several tests on the effect of sound speed to the 1-D simulations, and chose to fix the sound speed for the 2-D runs at 8.238×10^8 cm s^{-1}. This was the lowest value that didn't seem to change the dynamics of the system to a high degree, keeping in mind the ever-present computational time dilemna. Sound speeds within the bubble of ten times this fast ($\sim$ c/3) took ten times as long to run and looked pretty much the same.

The velocity through the bubble is proportional to the radius. The initial radius of the bubble is estimated by eyeballing the radio images of the remnant, but this alone is not reliable since we are not sure what exact stage in the evolution we are looking at. Therefore the bubble radius is varied in the simulations. The pressure in the bubble is also an input parameter in the simulations. The values of the pressure are expressed as a ratio to that just inside the inner shock, and range from .775 times that of the reverse shock to .0075 times. For reference, the pressure behind the reverse shock is $\sim$ 1.7 times the pressure behind the forward shock for a self-similar driven wave with s=0, n=9.

At its outer radius, the bubble has gathered some of the ejecta (γ=5/3) in its expansion into the unshocked ejecta. We assume the density here is four times the outer density, and the thickness is determined by how much material it has swept from the center. The velocity here is still proportional to the radius, and the pressure is the same as the bubble interior.

2.2. The Unshocked Ejecta

The unshocked ejecta, located between the central pulsar bubble and the reverse shock, is characterized by flat density and pressure profiles, and a velocity proportional to the radius. This ejecta plateau goes out to a radius close to where the reverse shock is located, where the density falls off as a power law ($\rho \propto r^{-9}$). The location of this plateau radius, together with the scaling for density, determines the mass of the ejecta in the supernova explosion. The pressure is chosen so that the local expansion velocity remains highly supersonic.

2.3. The Reverse Shock and Forward Shock

The reverse and forward shock pressure, density, and velocity profiles come from the solution for a self-similar driven wave (SSDW)(Chevalier 1982) with s=0, n=9, which is appropriate for Type II supernovae, those that produce pulsars. The s=0 corresponds to a flat density profile for the ambient medium, and the n=9 corresponds to a power law density profile of $\rho \propto r^{-9}$ of the expanding matter. For the 1-D simulations, the self-similar driven wave solution was calculated from a one-dimensional hydrodynamics simulation, and was then read in to the code and normalized to parameters appropriate to the Vela supernova remnant. For the two-dimensional simulations, we first ran a simulation of the SSDW with random noise added near the contact discontinuity to seed the instability. A detailed analysis of the generation of Rayleigh-Taylor instabilities in self-similar driven waves has been performed by Chevalier, Blondin, and Emmering (Chevalier, Blondin, and Emmering 1992). The fully evolved SSDW was used in the initial conditions for the 2-D runs, again normalized to appropriate values.

Outside the forward shock, the pressure is negligible compared to behind the blastwave, and the velocity is zero. It is also important to note that these simulations were done with an expanding grid, so the outer boundary follows the forward shock. This should be remembered especially when observing the figures in sections 3 and 4.

3. One-Dimensional Simulations

First a word on how the images were created and what they represent. The one-dimensional data sets are rendered as space-time diagrams, with space increasing from left to right, and time increasing from top to bottom. Since the grid is expanding, horizontal points at different times do not correspond to the same distance. Further, since the outer shock does not expand uniformly, one should not assume linear growth. Apparent jumps in the diagram may be due to the outer shock suddenly speeding up or slowing down. The density diagrams are simply colored by the logarithm of the density at each point. The other type of picture is intended to highlight regions where we would hope to see Rayleigh-Taylor instabilities in a two or three dimensional simulation. Using the simple principle that this type of instability occurs when low density gas accelerates higher density gas, we plot the density gradient multiplied by the pressure gradient divided by the density at each point. We expect that at points where this quantity is negative, the instability can occur, and with more negative numbers, the instabilities should become more defined. Color images of these 1D simulations are available at http://wonka.physics.ncsu.edu/ dmfriers/stime.html.

3.1. Varying Pressure

The first simulation we ran was of the reverse shock and forward shock, without a bubble in the center, for comparison. The reverse shock eventually bounces off of the center and makes its way back outwards.

The simulations with the bubble have many elements in common. All have the bubble shock moving outwards in the space-time diagram, which means that it is moving faster than the outer shock. Further, the rate at which it moves out depends on the pressure ratio. This shock then hits the reverse shock, sending transmitted and a reflected wave toward and away from the center. The wave moving toward the center is stronger, and carries material into the bubble. The bubble compresses, and eventually turns the material around before it touches the center. The material then bounces back and forth, never reaching any closer to the center. For these simulations, there are patches where we would see instabilities around the interaction between the reverse shock and the bubble, most defined at the time when the pulsar bubble is compressed the most. However, at no time are the areas predicting the instability as strongly defined as in the vicinity of the reverse shock falling into the unshocked ejecta.

As we change the pressure ratios, the closest distance that the reverse shock material gets to the center increases with the bubble pressure. The chances of an instability forming does not seem to be greatly associated with the bubble pressure, only the distances at which these instabilities would occur. One possible problem is that even at the highest pressure ratio that we tried, the bubble pressure is still much smaller than what was predicted in Section 2.1.

3.2. Varying Bubble Size

Noting that the pressure behind the reverse shock was dropping off rapidly with time, and the collisions between the reverse shock and the bubble shock did not seem to be as big as expected, we tried starting the bubble shock at a larger radius at the beginning of the simulation. This also would aid the problem of the bubble pressure being too high, because the total energy per unit volume is spread out over a larger volume. In the simulations described above, the radius of the bubble was set as one fourth of the outer radius. We then ran simulations with the bubble radius one half and one third the outer radius. In these, we found similar results as the previous. The density diagrams in some cases looked more mixed up, but in general the effects were minimal.

3.3. Varying Bubble Sound Speed

Unfortunately, while running multi-dimensional computer simulations, computational time is often a problem, even on the fastest supercomputers. Since the run time is determined by the fastest sound speed on the grid, which is almost always inside the bubble for these simulations, we investigate the effect of bubble sound speed on the dynamics of the system before moving on to 2-D. The expression for sound speed is

$$v_{sound} = \sqrt{\gamma P/\rho}$$

where γ is the equation of state adiabatic index, P is pressure, and ρ is density. We examine the effect of sound speed by changing the density within the bubble. As previously stated, the actual sound speed within the bubble is expected to be c/3. We ran tests with sound speeds of 8.238×10^{7} cm s^{-1}, 8.238×10^{8} cm s^{-1}, and 8.238×10^{9} cm s^{-1}. With larger sound speeds, the pulsar bubble is

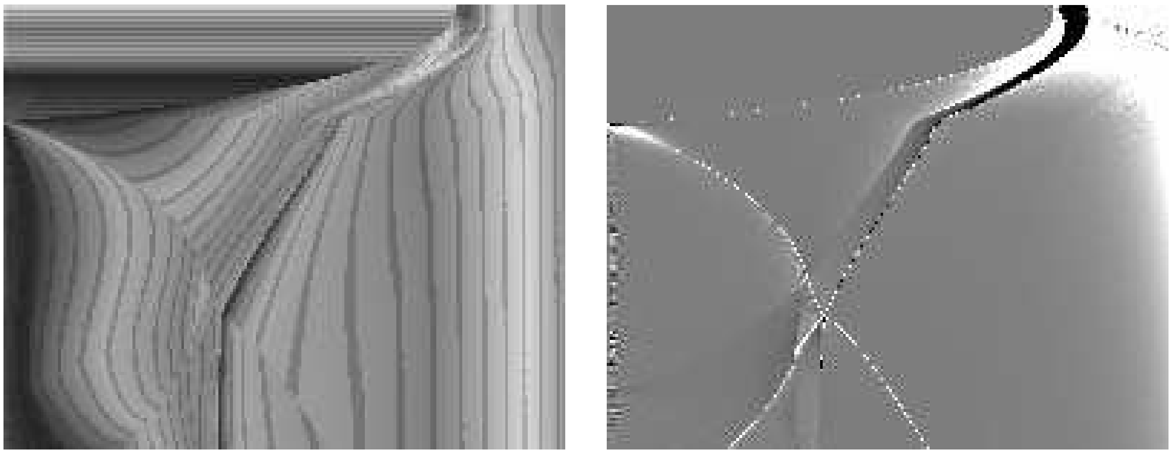

Fig. 1.— Space-Time diagrams of the 1D simulation without a pulsar bubble. On the left is the gas density, on the right is the product of the density and pressure gradients. Black on this figure represents an unstable region, while shock fronts show up in white.

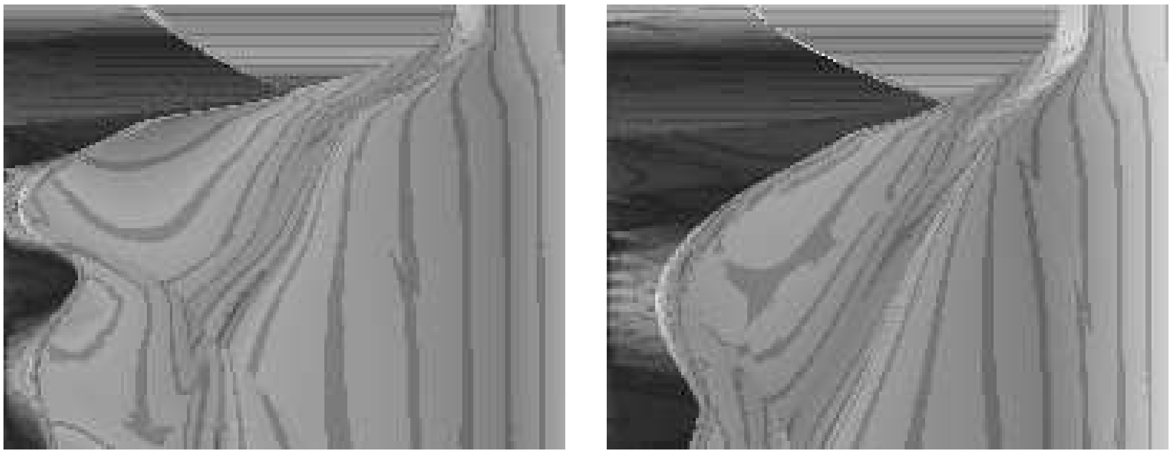

Fig. 2.— Effects of varying bubble pressure can be seen by comparing these 1D simulations. The bubble on the right starts off with a pressure comparable to the pressure behind the reverse shock at the beginning of the simulation. The bubble on the left starts off with a pressure 100 time lower.

compressed more. However for the latter two runs, the overall dynamics remain about the same, while the third took approximately ten times longer than the second. Therefore we fix the sound speed at 8.238×10^8 cm s^{-1} for the 2-D runs.

4. Two-Dimensional Simulations

4.1. First attempt

The goal of this work is to investigate the possibility that dynamical instabilities may be the origin of the filamentary structure seen in the interior of the Vela supernova remnant. To this end we begin by running a preliminary simulation in 2D on a relatively high-resolution moving cylindrical (r-z) grid of 1000^2 zones. All of the initial structures for this simulation are spherically symmetric - nothing is done to seed any instabilities. The first instability to develop is the convective instability associated with the contact discontinuity of the self-similar driven wave. The second instability is a Richtmeyer-Meshkov instability as the reverse shock crashes through the dense shell of swept gas surrounding the pulsar bubble. Finally, there may be another Rayleigh-Taylor instability as the reverse shock comes back out from the center, accelerating the already clumpy pulsar bubble shell. All three of these instabilities can be seen in the two snapshots from the 2D simulation shown in Figure 5.

The main concern with the morphology of this run was that the bubble was entirely crushed. The interaction region where we expect the filamentary structure to be present appears to be too small in comparison with outer radius, which was not necessarily observed in the 1-D simulations. We increase the pressure inside the bubble in subsequent runs to try to alter this.

4.2. Second attempt

The first 2-D simulation was run over Christmas break on the N.C. State Astrophysics Group's SGI Octane workstation. Since it took over two weeks to run, we were forced to cut the resolution in half for the next two 2-D runs. This second run adds the evolved self-similar driven wave in the initial conditions, and raises the pressure in the bubble by a factor of 10.

Despite the raised pressure, again the bubble is completely crushed. We increase both the pressure inside the bubble and the bubble radius in the next simulation to see how this affects the bubble.

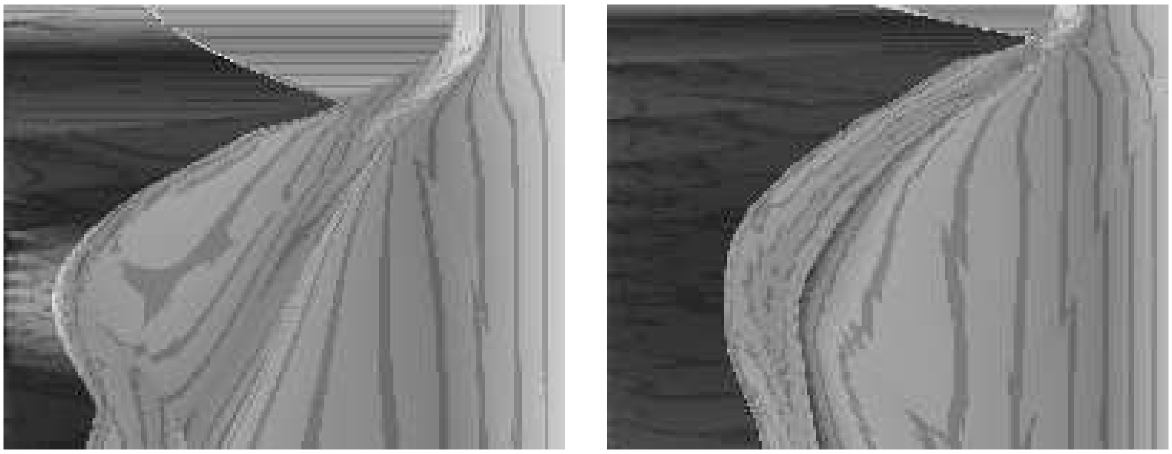

Fig. 3.— Effects of varying the initial bubble radius can be seen by comparing these 1D simulations. Both have the same bubble (relatively high) bubble pressure, but the simulation on the right starts off with a bubble radius twice that of the simulation on the left.

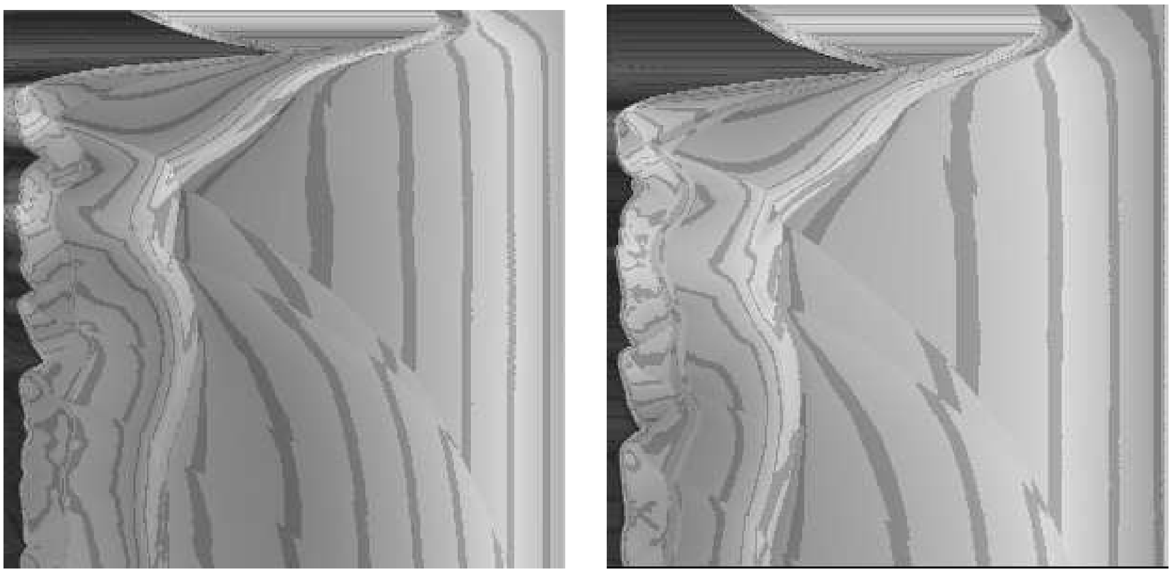

Fig. 4.— The effect (or lack thereof) of varying the sound speed within the bubble can be seen from comparing these 1-D simulations. The simulation on the left has sound speed one-tenth of that on the right. The right simulation took approximately ten times more time steps.

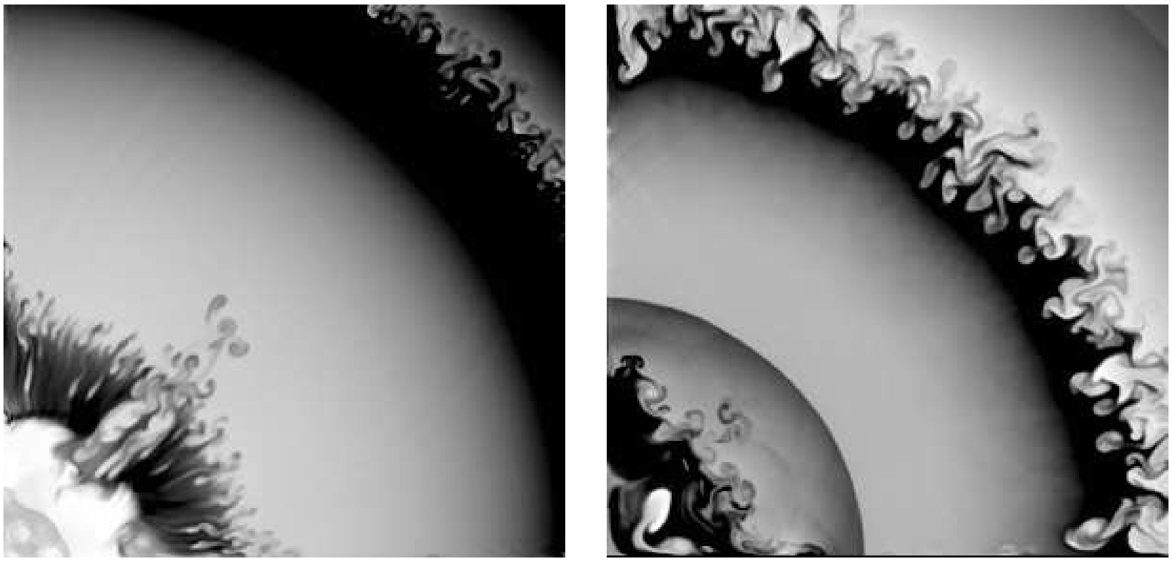

Fig. 5.— Two-Dimensional simulation of the SNR/Pulsar nebula interaction. The left image is just after the reverse shock has reflected off the center. The right image is shortly afterward, once the reverse shock has passed back through the pulsar nebula shell. In both images the Rayleigh-Taylor fingers of dense gas seen in the upper right-hand corner is the unstable interface in the self-similar driven wave. Nothing was done to "seed" any of the instabilities present in this simulation. The forward shock is off at much larger radii.

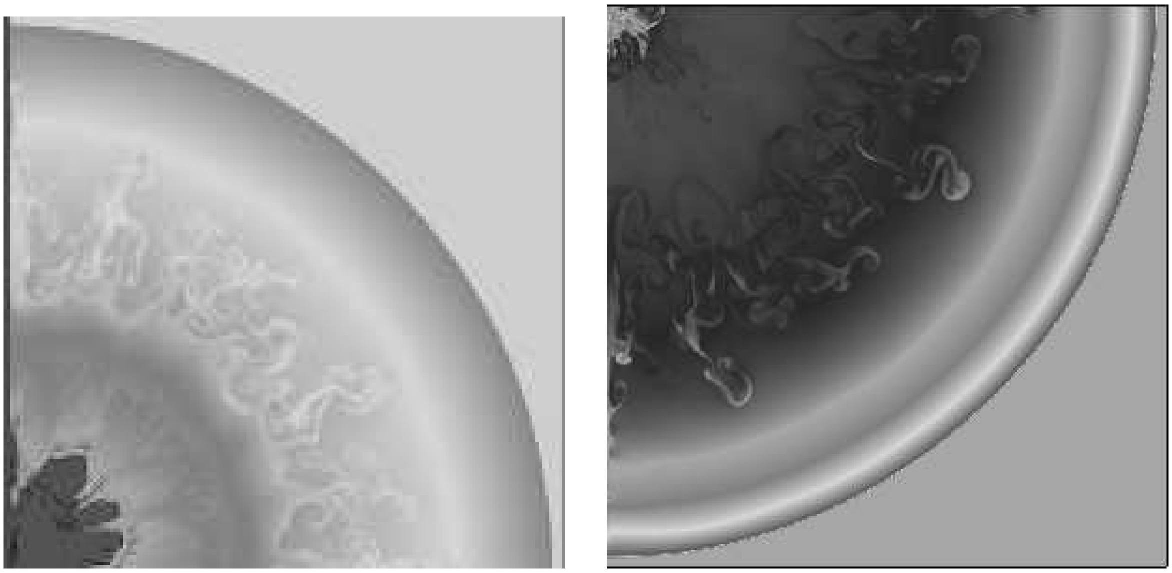

Fig. 6.— Second 2-D run (pressure is higher in the center and evolved SSDW is added). These images are of the entire simulation; the outer shock is the outermost circle. The left image is just before the reverse shock hits the center, and the right image is a short time after it hits. Ignore the fact that they're pointing in opposite directions. Notice the bubble is totally crushed.

4.3. Third attempt

In order to see if it is possible for the bubble not to be crushed, we increase the pressure in the bubble by another factor of 10, and double the size of the bubble. The bubble makes a valiant attempt at turning back the reverse shock, slowing it down some. However, the reverse shock floods in from the sides (possibly due to edge effects) and eventually squashes almost the entire bubble again. We are currently a simulation at twice this resolution with the same parameters. This will allow us to see how resolution affects the morphology of the system, as well as whether this will prevent the bubble from being crushed.

Another way to determine how much the bubble is destroyed is by examining plots of gamma. After the reverse shock hits the center in this simulation, almost all points on the grid have $\gamma = 5/3$. A few points in the lowest density areas have $\gamma \sim 1.5$.

5. Synchrotron modeling

It is important to keep in mind while viewing these visualizations that the plots are of density, which is not necessarily at all like the synchrotron emissions that are observed. In order to do accurate synchrotron approximations, information about the strength and direction of the magnetic field and the population of relativistic electron is needed. However this is not possible with only the density, pressure, and velocity at certain times, so we derive an approximation formula for synchrotron emissivity based on these quantities.

5.1. Theoretical basis

First, we assume turbulent amplification of the magnetic field, so

$$B^2 \propto P$$

where P is pressure. We also assume (not so good an assumption) that the relativistic electron density varies due to the adiabatic compression or expansion with a ratio of specific heats of 4/3. These two approximations give:

$$emissivity(ergcm^{-3}s^{-1}Hz^{-1}sr^{-1}) \propto P^{(1+\alpha)/2}\rho^{(3+2\alpha)/3}$$

where α is the radio spectral index of the pulsar bubble, $S_\nu \propto \nu^{-\alpha}$. The radio spectral index for the Vela X region has been shown to be $\alpha = 0.16$ (citedwa91). Another assumption that can be made is that the relativistic electrons are confined to the area where $\gamma = 4/3$. We use a linear interpolation for the areas where gamma has been mixed. Since we're only considering relative intensities, the proportionality constants can be thrown away. Therefore our final model for the synchrotron emissivity is:

$$emissivity = (5 - 3\gamma) \times P^{0.58} \times \rho^{1.107}$$

We use a line of sight integration routine to generate a sample observable picture. Here are some of those pictures from the final two-dimensional run (with high pressure in the bubble and larger bubble size).

5.2. Synchrotron pictures

The first picture (fig. 8a.) is a synchrotron visualization of the initial conditions of the final 2D run. The second picture (fig. 8b.) is 2500 time steps later, when the reverse shock has just hit the bubble shock. The third image (fig. 9a.) is 2500 time steps after this, as the bubble is getting very compressed. It is still mostly spherical in the density plots at this point. The fourth image (fig. 9b.) is 1500 time steps later, when the bubble appears to be turning back the reverse shock a little bit. By the time of the fifth image (fig. 10a., 1000 time steps later), material has begun to flow in from the sides. This image corresponds to the density plot shown in figure 7a. The sixth image (fig. 10b.) is 2500 time steps later, when almost all of the low density area has been eliminated. This image is taken from the same time step as the density plot of figure 7b.

It appears that figures such as 9b. and 10a. might be roughly what we are seeing in the Vela remnant. To further test this, we need to try a higher resolution run (currently in progress) and test the synchrotron visualization routine more.

6. Results, Questions

Future plans: evolved bubble. Passive magnetic field to aid synchrotron visualizations.

REFERENCES

Bock, D. C.-J., Turtle, A. J., and Green, A. J. 1998, AJ, 116, 1886.

Chevalier, R. A. 1982, ApJ, 258, 790.

Chevalier, R. A., Blondin, J. M., and Emmering, R. T. 1992, ApJ, 392, 118.

Collela, P., and Woodward, P. R. 1984, J. Comp. Phys., 54, 174.

Dwarakanath, K.S. 1991, Journ. of Astrophys. and Astron., 12, 199.

Frail, D. A., Bietenholz, M. F., Markwardt, C. B., and Ögleman, H. 1997, ApJ, 475, 224.

Hester, J. J., Stone, J. M., Scowen, P. A., Jun, B.-I., Gallagher, J. S., III, Norman, M. L., Ballester, G. E., Burrows, C. J., Casertano, S., Clarke, J. T., Crisp, D., Griffiths, R. E., Hoessel, J. G., Holtzman, J. A., Krisp, J., Mould, J. R., Sankrit, R., Stapelfeldt, K. R., Trauger, J. T., Watson, A., and Westphal, J. A. 1996, ApJ, 456, 225.

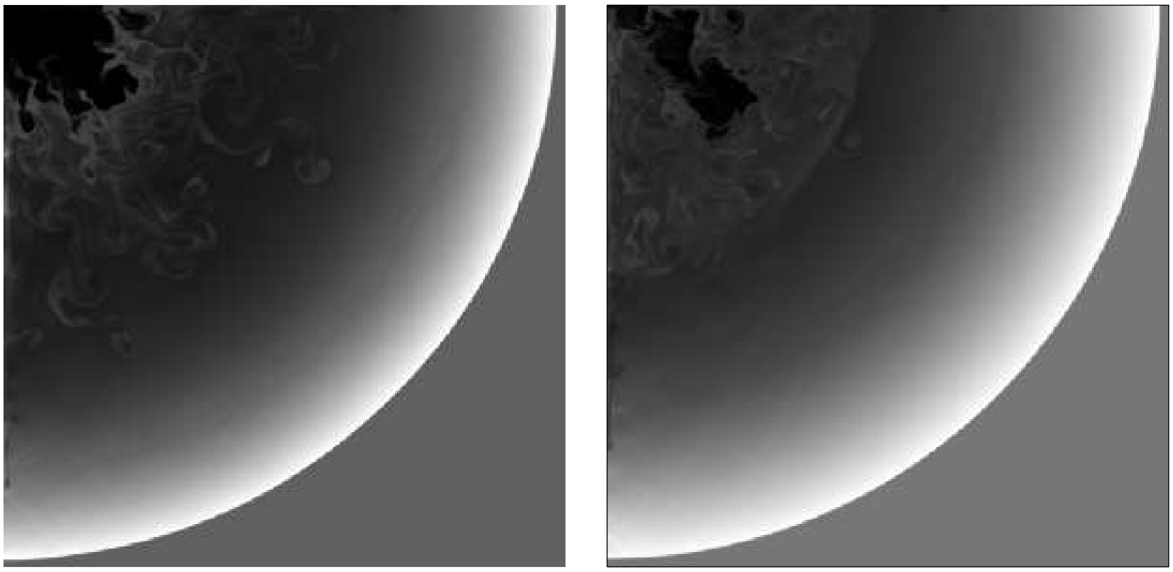

Fig. 7.— Third 2-D run (higher pressure in the center and larger initial bubble size). The black area is the bubble. The picture on the left shows fingers poking in at the bubble. The picture on the right shows that these fingers eventually crush the bubble from the sides.

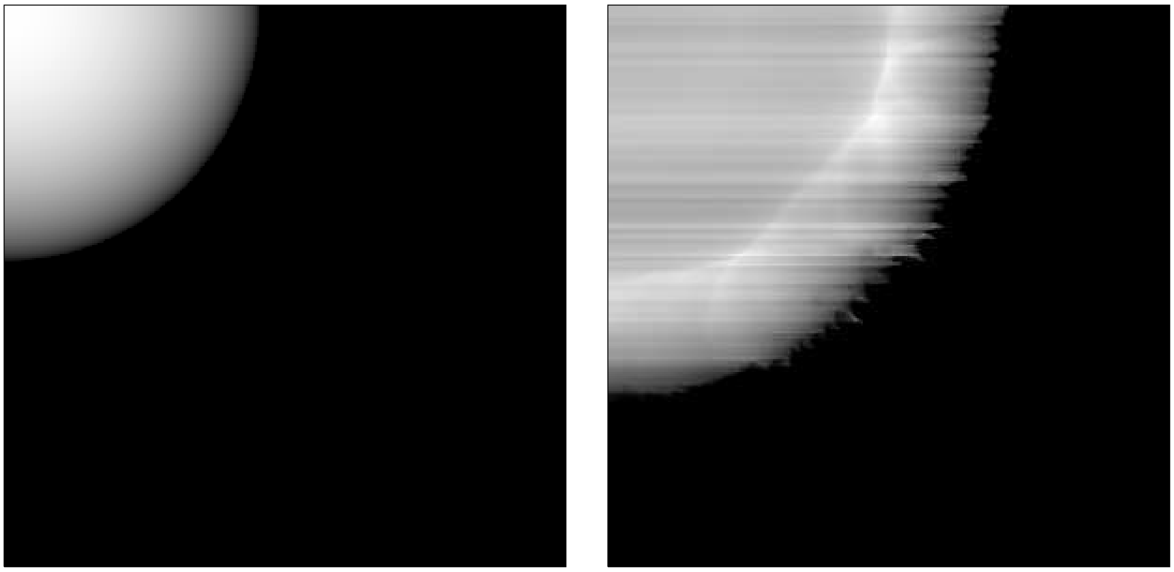

Fig. 8.— The figure on the left is a sample synchrotron visualization of the initial conditions of the final 2d run. The figure on the right is 2500 time steps later, just as the reverse shock hits the bubble shock.

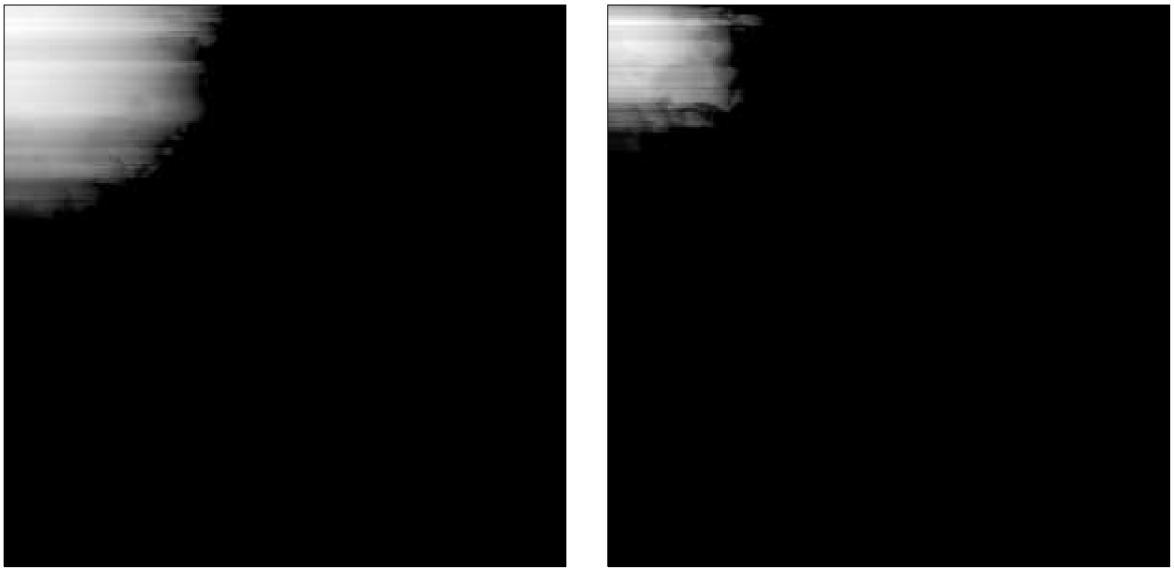

Fig. 9.— The figure on the left is another synchrotron visualization of the final 2D run, 2500 time steps after figure 8b. On the right is 1500 time steps after this.

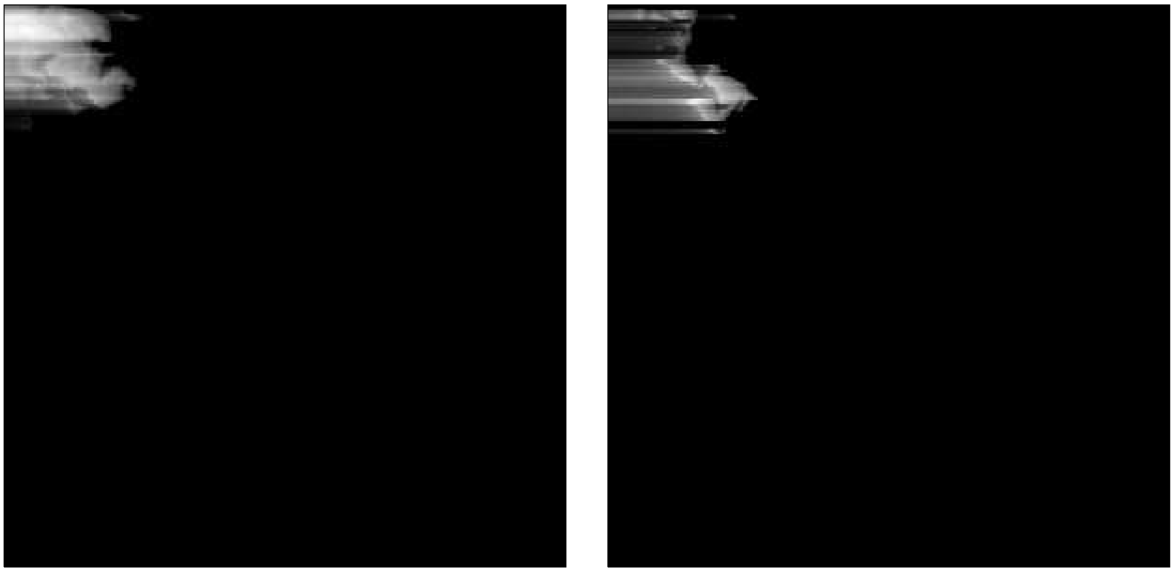

Fig. 10.— The figure on the left is another synchrotron visualization of the same run, 1000 time steps after the previous. This picture corresponds to figure 7a. On the right is 2500 time steps after this. This corresponds to figure 7b.

Jun, B.-I. 1998, ApJ, 499, 282.

Markwardt, C. B., and Ögleman, H. B. 1997, ApJ, 480, L13.

Markwardt, C. B., and Ögleman, H. 1995, Nature, 375, 40.

Reynolds, S. P., and Chevalier, R. A. 1983, ApJ, 278, 630.

Weiler, K. W., and Panagia, N. 1980, Astronomy and Astrophysics, 90,269.

Wijers, R. A. M. J., and Sigurdsson, S. 1997, Monthly Notices of the Royal Astronomical Society, 290, 276.

Table 1. Input parameters for the final 2D run.

Parameter name	Value
Run name	vela2
Zones	1000×1000
Outer radius	1.51×10^{19} cm
Starting time	2.528596×10^{10} s
Outer velocity	$\sim 4 \times 10^{8}$
Bubble radius	$.5 \times$ outer radius
Pressure ratio of the bubble	7.75×10^{-1}
Ambient density	4.364×10^{-25} gm cm^{-3}
Bubble density	$.04 \times$ ambient density
Number of time steps run	20,000